Predictive Control for Visual Servo Stabilization of Nonholonomic Mobile Robots

CAO Zheng-Cai[1, 2] YIN Long-Jie[1] FU Yi-Li[3] LIU Tian-Long[1]

Abstract Visual servo stabilization of nonholonomic mobile robots has gained extensive attention. However, currently, the solution of the problem does not consider both the visibility constraints and the actuator limitations, so the designed controller is difficult to realize satisfactory performance in practical application. In this paper, a predictive controller for the visual servo stabilization of a mobile robot is presented. Firstly, a kinematic predictive stabilization controller utilized to generate the command of velocity is introduced. Then, in order to make the actual velocity of the mobile robot asymptotically approach to the desired one, a dynamic predictive controller is designed. The proposed predictive controller can deal with the constraints easily. Finally, several simulations are performed, and the results illustrate that the proposed control scheme is effective to solve the visual servo stabilization problem.

Key words Nonholonomic mobile robots, visual servo stabilization, predictive control, constraints

Citation Cao Zheng-Cai, Yin Long-Jie, Fu Yi-Li, Liu Tian-Long. Predictive control for visual servo stabilization of nonholonomic mobile robots. *Acta Automatica Sinica*, 2013, **39**(8): 1238−1245

DOI 10.3724/SP.J.1004.2013.01238

In recent years, the use of visual feedback for motion control of nonholonomic mobile robots (NMR) has received wide attention and is a topic of great research interest. Many studies have been carried out in this field and can be divided into two main portions: visual tracking and visual stabilization. In this paper, we consider the problem of visual servo stabilization of a nonholonomic mobile robot with a monocular vision system onboard. The basic idea is using visual information to drive the mobile robot from an initial pose to the desired one, which is given by an image previously taken at the desired pose. From the point of view of control, the visual stabilization problem is more challenging than the visual tracking problem of NMR, because nonholonomic systems cannot be asymptotically stabilized by any time-invariant continuous state feedback control law. During the past decade, several control strategies have been presented to obtain satisfactory control performance for nonholonomic systems[1−3]. However, these techniques cannot take the vision system into the feedback loop, and it is assumed that full state feedback is available, which is clearly not true for visual servoing systems because of unknown depth information.

For the visual servo stabilization of NMR, much work has been done. A traditional approach is to perform the motion by computing the epipolar geometry between the current image and the target one[4−6], but the estimation of the epipolar geometry becomes ill conditioned for planar scenes, which are quite usual in human environments. A good alternative is the homography-based approach[7−8], but the homography model is not well defined if there is no dominant plane in the scene or the feature points are not coplanar. In [9], a switching controller based on the epipolar geometry and the homography was proposed, which avoided the drawbacks of each one and allowed a smooth motion of the robot. Another feasible way is to use the trifocal tensor[10]. Recently, Zhang et al.[11] presented a hybrid visual servo stabilization strategy based on a motion-estimation technique, which can be applied in both planar and nonplanar scenes and requires no matrix estimation or decomposition. In [12], a robust stabilization controller based on a two-phase technique was presented, which can stabilize the mobile robot to the origin even though the depth information and precise visual parameters were lacking. The above cited works, however, only take the mobile robot kinematics into account. There have been few researches where the dynamics of the mobile robot is considered to achieve the visual servo stabilization. In [13], an adaptive sliding-mode dynamic stabilizing controller was proposed for an uncertain nonholonomic dynamic mobile robot when the camera was fixed to the ceiling. In [14], a dynamic feedback control law based on backstepping technique was presented for a wheeled mobile robot to perform the position-based visual stabilization.

In summary, the aforementioned approaches are of important reference in visual servo stabilization of mobile robots. However, these control schemes do not take the visibility constraints and the actuator limitations in velocity and torque into account in the controller design, so the visual data obtained from the camera may get lost, which often leads to the failure of servoing. Recently, Allibert et al.[15] proposed an image-based visual servoing for a 6 degrees of freedom free-flying camera via nonlinear model predictive control which can easily deal with the 2D and 3D constraints. Compared with the free-flying camera, mobile robots have much larger working space and present complex nonholonomic dynamics, which make it more difficult for mobile robots to keep the target in the field of view.

In this paper, considering the robot kinematics and dynamics, asymptotic stabilization of the pose of a nonholonomic mobile robot with a monocular camera fixed onboard is achieved by exploiting the visual predictive control strategy benefit from the work given in [15]. By using the nonlinear model predictive control approach, the visibility constraints, velocity limitations, and torque limitations can be taken into account in the controller design easily. The design of the controller is divided into two parts, each part being a controller itself. The first one is presented for the kinematic model, the other one is applied to the dynamic model. The simulation results show that the proposed predictive controller not only is capable of driving the mobile robot to the desired pose, but also can make the target

Manuscript received July 19, 2012; accepted December 20, 2012
Supported by International Science and Technology Cooperation Program (2011DFG13000), Open Foundation of State Key Lab of Fluid Power Transmission and Control of China (GZKF-201212), Fundamental Research Funds for Central Universities of China (ZZ1222), and Key Laboratory of Advanced Engineering Surveying of NASMG of China (TJES1106)
Recommended by Associate Editor TAN Min
1. College of Information Science and Technology, Beijing University of Chemical Technology, Beijing 100029, China 2. Key Laboratory of Embedded System and Service Computing, Ministry of Education, Tongji University, Shanghai 201804, China 3. State Key Laboratory of Robotics and Systems, Harbin Institute of Technology, Harbin 150080, China

always remain visible.

This paper is organized as follows. In Section 1, the nonholonomic mobile robot model, camera model, and robot-camera-target model are introduced. In Section 2, the visual servo stabilization problem is stated. Then the proposed control algorithm is developed in Section 3. Simulation results are given in Section 4. Finally, Section 5 concludes the paper.

1 Mathematical modeling

In this section, the nonholonomic mobile robot model and the camera model are first briefly introduced. Then, a robot-camera-target model is presented. These models are key to the development of our controller.

1.1 Nonholonomic mobile robot model

As shown in Fig. 1, the mobile robot with two independently driven wheels is used, and a monocular camera is fixed on board. O-XYZ is the world coordinate system, o-$x_r y_r$ is the coordinate system fixed to the robot, and C-$x_c y_c z_c$ is the camera coordinate system. The mass center o of the robot is located at the middle of the driving wheels. The camera is fixed along the y_r axis, and the distance from C to o is l. r is the radius of rear wheels and $2L$ is the distance between rear wheels.

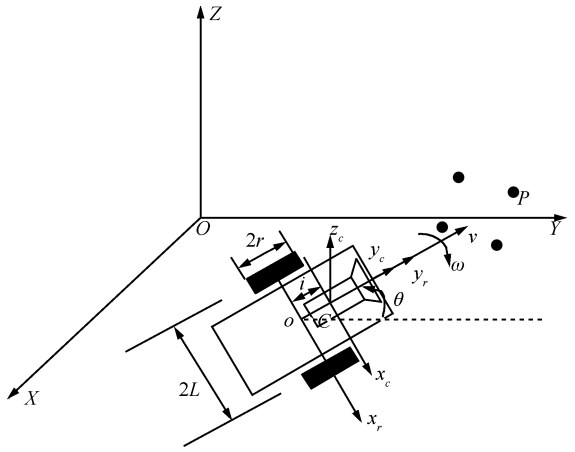

Fig. 1 Mobile robot with monocular camera

The kinematic model for the mobile robot under the nonholonomic constraints of pure rolling and non-slipping can be expressed in accordance with the frame defined in Fig. 1 as follows:

$$\dot{\boldsymbol{q}} = \begin{bmatrix} \dot{x}(t) \\ \dot{y}(t) \\ \dot{\theta}(t) \end{bmatrix} = \begin{bmatrix} -\sin\theta(t) & 0 \\ \cos\theta(t) & 0 \\ 0 & 1 \end{bmatrix} \begin{bmatrix} \nu(t) \\ \omega(t) \end{bmatrix} \tag{1}$$

where $\boldsymbol{q} = [x, y, \theta]^{\mathrm{T}}$ is the state of the mobile robot, with $x(t)$, $y(t)$ being the coordinates of o, and $\theta(t)$ the orientation angle of the mobile robot. Additionally, $\nu(t)$ and $\omega(t)$ are linear and angular velocities of the mobile robot, respectively.

Assuming all the uncertainties and disturbances are zero, the dynamic equation[16] of simple model of the mobile robot can be described as

$$\bar{\boldsymbol{M}}(\boldsymbol{q})\dot{\boldsymbol{\nu}} = \bar{\boldsymbol{B}}\bar{\boldsymbol{\tau}} \tag{2}$$

where $\bar{\boldsymbol{\tau}} = [\tau_l, \tau_r]^{\mathrm{T}}$ consists of motor′s torque τ_l and τ_r, which act on the left and right wheels, respectively. $\boldsymbol{\nu} = [\nu, \omega]^{\mathrm{T}}$ represents the velocity vector.

Assuming $\tau_1 = (\tau_l + \tau_r)/r$, $\tau_2 = L(\tau_l - \tau_r)/r$, the dynamic equation (2) becomes

$$\bar{\boldsymbol{M}}(\boldsymbol{q})\dot{\boldsymbol{\nu}} = \boldsymbol{\tau} \tag{3}$$

where $\boldsymbol{\tau} = [\tau_1, \tau_2]^{\mathrm{T}}$ denote linear and angular torques, respectively, which act on the body of the mobile robot. $\bar{\boldsymbol{M}}$ and $\bar{\boldsymbol{B}}$ are selected as

$$\bar{\boldsymbol{M}} = \begin{bmatrix} m & 0 \\ 0 & I \end{bmatrix} \bar{\boldsymbol{B}} = \frac{1}{r} \begin{bmatrix} 1 & 1 \\ L & -L \end{bmatrix} \tag{4}$$

with m being the mass of the body and I the moment of inertia of the body about the vertical axis through o.

1.2 Camera model

The camera model shows the projective relationship between the target point in the 3D Euclidean space and its corresponding point in the image plane. As shown in Fig. 1, considering four static feature points in the scene as the target, based on the perspective model[5], one can obtain

$$\begin{cases} u = fk_u \dfrac{x_c}{y_c} + u_0 \\ \upsilon = fk_\upsilon \dfrac{z_c}{y_c} + \upsilon_0 \end{cases} \tag{5}$$

where $(x_c, y_c, z_c)^{\mathrm{T}}$ is the 3D coordinate of feature point P with respect to the camera frame, $(u, \upsilon)^{\mathrm{T}}$ is the corresponding image pixel coordinate, f is the focal length of the camera, k_u, k_υ are the number of pixels per unit distance in image coordinates, and $(u_0, \upsilon_0)^{\mathrm{T}}$ is the coordinate of the principal point in pixels.

Based on (5), the following 2D image coordinate $\boldsymbol{p} = [\ p_x \quad p_y]^{\mathrm{T}}$, which will be further used in the control development, can be obtained:

$$\begin{bmatrix} p_x \\ p_y \end{bmatrix} = \begin{bmatrix} f\dfrac{x_c}{y_c} \\ f\dfrac{z_c}{y_c} \end{bmatrix} = \begin{bmatrix} \dfrac{u - u_0}{k_u} \\ \dfrac{\upsilon - \upsilon_0}{k_\upsilon} \end{bmatrix} \tag{6}$$

1.3 Robot-camera-target model

The robot-camera-target model describes the dynamic relationship among the robot, camera and target. Based on the geometric analysis for the coordinate systems shown in Fig. 1, one can get

$$\begin{cases} a = x_r \cos\theta - y_r \sin\theta + x \\ b = x_r \sin\theta + y_r \cos\theta + y \\ x_r = x_c \\ y_r = y_c + l \end{cases} \tag{7}$$

where (a, b) and (x_r, y_r) are the coordinates of point P with respect to the world coordinate system and the robot coordinate system, respectively. Clearly, a and b are constants.

Taking the time derivative of (7) and using (1), the robot-camera-target model can be obtained as follows:

$$\begin{cases} \dot{x}_c = y_c\omega + l\omega \\ \dot{y}_c = -\nu - x_c\omega \\ \dot{\theta} = \omega \end{cases} \tag{8}$$

2 Problem statement

In general, the visual servo stabilization can be regarded as using visual information to control a mobile robot to a desired pose, which is specified by an image of the observed target previously taken at the goal position. Therefore,

when the mobile robot is stabilized to the desired pose, the current and desired images will be the same.

Define the image coordinate of feature point P in the desired image to be $\boldsymbol{p}_d = [p_{xd}, p_{yd}]^{\mathrm{T}}$, and θ_d the desired orientation of the mobile robot. To facilitate the subsequent development of our controller, the following coordinate transformation is introduced:

$$\boldsymbol{s} = \begin{bmatrix} s_1 \\ s_2 \end{bmatrix} = \begin{bmatrix} \dfrac{p_x}{p_y} \\ -\dfrac{f}{p_y} \end{bmatrix}, \boldsymbol{s}_d = \begin{bmatrix} s_{1d} \\ s_{2d} \end{bmatrix} = \begin{bmatrix} \dfrac{p_{xd}}{p_{yd}} \\ -\dfrac{f}{p_{yd}} \end{bmatrix} \tag{9}$$

Then the following composite error vector including both image signals and orientation is defined:

$$\boldsymbol{e} = \begin{bmatrix} e_1 \\ e_2 \\ e_3 \end{bmatrix} = \begin{bmatrix} s_1 \\ s_2 \\ \theta \end{bmatrix} - \boldsymbol{T}_e \begin{bmatrix} s_{1d} \\ s_{2d} \\ \theta_d \end{bmatrix} \tag{10}$$

where

$$\boldsymbol{T}_e = \begin{bmatrix} \cos\theta_e & -\sin\theta_e & 0 \\ \sin\theta_e & \cos\theta_e & 0 \\ 0 & 0 & 1 \end{bmatrix} \tag{11}$$

with $\theta_e = \theta - \theta_d$, which can be estimation based on the motion-estimated technique[11].

It can be observed from (10) and (11) that when the error $\boldsymbol{e} \to 0$, one can obtain

$$s_1 \to s_{1d}, s_2 \to s_{2d}, \theta \to \theta_d \tag{12}$$

Based on (9) and (12), the image coordinate $p_x \to p_{xd}$, $p_y \to p_{yd}$, and $\theta_e \to 0$, that is, the current and desired images are the same, the mobile robot reaches the desired pose.

Therefore, the objective of the visual servo stabilization is to design a controller $\boldsymbol{\tau} = [\tau_1, \tau_2]^{\mathrm{T}}$ to obtain $\lim_{t\to\infty}\boldsymbol{e} = 0$ and $\lim_{t\to\infty}\boldsymbol{\tau} = 0$.

Additionally, to ensure the target remains in the camera′s field-of-view during the servoing process and the mobile robot moves safely with a high velocity, two kinds of constraints are considered in the controller design as follows:

1) Visibility constraints, such as limitations in image pixel coordinate, which can keep the visual features always visible

$$\begin{cases} u_{\min} \le u(t) \le u_{\max} \\ v_{\min} \le v(t) \le v_{\max} \end{cases} \tag{13}$$

2) Control constraints, such as actuator limitations in velocity and torque

$$\begin{cases} \boldsymbol{\nu}_{\min} \le \boldsymbol{\nu}(t) \le \boldsymbol{\nu}_{\max} \\ \boldsymbol{\tau}_{\min} \le \boldsymbol{\tau}(t) \le \boldsymbol{\tau}_{\max} \end{cases} \tag{14}$$

To handle the constraints, nonlinear model predictive control (NMPC) is applied to design the controller as described in Section 3.

3 Predictive controller design

Due to the capability of constraint handling, NMPC, which is an optimal control strategy, has become an increasingly popular control technique used in industry. The control problem is stated as a nonlinear constrained optimization problem. The behavior of the system is predicted based on the system model over a predictive horizon at each sampling time. Then, using the predicted information, a future sequence of control input is obtained by minimizing the objective function. Only the first control input of the optimal control sequence is used. The same procedure is repeated using the updated measurements and a shifted horizon at the next sampling time. A more comprehensive explanation of NMPC can be found in [17].

The extension of NMPC to visual servoing is named as visual predictive control. In this section, based on NMPC, a visual predictive stabilization controller, which consists of the kinematic and dynamic controllers, is designed to ensure that the mobile robot can be driven to the desired pose while keeping the feature points always visible during the visual servo process.

3.1 Kinematic controller

The kinematic controller is designed for the kinematic model of the mobile robot. Substituting (6), (8), and (9) for the time derivative of (10), the following error dynamic model can be obtained:

$$\dot{\boldsymbol{e}} = \begin{bmatrix} \dot{e}_1 \\ \dot{e}_2 \\ \dot{e}_3 \end{bmatrix} = \begin{bmatrix} -\omega e_2 + \omega l\alpha \\ \nu\alpha + \omega e_1 \\ \omega \end{bmatrix} \tag{15}$$

where $\alpha := 1/z_c$ is constant due to the planar motion of the mobile robot, and we assume that the height of feature point in the camera frame is not equal to zero, that is, $z_c \neq 0$.

Applying the Euler approximation to (15), the following discrete-time nonlinear error system can be obtained:

$$\begin{aligned} \boldsymbol{e}(k+1) = & \begin{bmatrix} e_1(k+1) \\ e_2(k+1) \\ e_3(k+1) \end{bmatrix} = \\ & \begin{bmatrix} e_1(k) - T\omega(k)e_2(k) + T\omega(k)l\alpha \\ e_2(k) + T\nu(k)\alpha + \omega(k)e_1(k) \\ e_3(k) + T\omega(k) \end{bmatrix} \end{aligned} \tag{16}$$

where T is the sampling period, and (16) can be rewritten in a compact representation as

$$\boldsymbol{e}(k+1) = f(\boldsymbol{e}(k), \boldsymbol{\nu}(k)) \tag{17}$$

By creating a nonlinear discrete-time model (17) of the error system, it is possible to use NMPC to control it. The approach is to find the control inputs that minimize the quadratic objective function by using a sequence quadratic program (SQP). The quadratic objective function of the system error and control input with a predictive horizon N_p is given by

$$\begin{aligned} J(k) = & \sum_{j=1}^{N_p} \boldsymbol{e}^{\mathrm{T}}(k+j|k)\boldsymbol{Q}\boldsymbol{e}(k+j|k) + \\ & \sum_{j=1}^{N_c} \boldsymbol{\nu}^{\mathrm{T}}(k+j-1|k)\boldsymbol{R}\boldsymbol{\nu}(k+j-1|k) \end{aligned} \tag{18}$$

where N_c is the control horizon, $\boldsymbol{Q}$ and $\boldsymbol{R}$ denote symmetric positive definite weighting matrices. The notation $(k+j|k)$ represents the prediction made at instant k of a value at instant $k+j$.

Based on (17), the prediction model can be obtained as follows:

$$\boldsymbol{e}(k+j|k) = f(\boldsymbol{e}(k+j-1|k), \boldsymbol{\nu}(k+j-1|k)), j \in [1, N_p] \tag{19}$$

Using (6), (9), and (10), the value of the system error measured at the current instant can be obtained as follows:

$$\boldsymbol{e}(k|k) = \begin{bmatrix} e_1(k|k) \\ e_2(k|k) \\ e_3(k|k) \end{bmatrix} = \begin{bmatrix} \dfrac{k_u(u(k|k)-u_0)}{k_v(v(k|k)-v_0)} - s_{1d}\cos(\theta_e(k|k)) + s_{2d}\sin(\theta_e(k|k)) \\ \dfrac{-fk_v}{v(k|k)-v_0} - s_{1d}\sin(\theta_e(k|k)) - s_{2d}\cos(\theta_e(k|k)) \\ \theta_e(k|k) \end{bmatrix} \tag{20}$$

In addition, the visibility constraints in (13) and velocity limitations in (14) are considered to ensure the feature points remain visible and the mobile robot moves safely with a high velocity.

Consequently, the kinematic predictive stabilization controller can be written as

$$\boldsymbol{\nu}^* = \arg\min_{\boldsymbol{\nu}} J(k) \tag{21}$$

s.t.

$$\begin{cases} \boldsymbol{e}(k|k) = \boldsymbol{e}_0 \\ \boldsymbol{e}(k+j|k) = f(\boldsymbol{e}(k+j-1|k), \\ \qquad\qquad \boldsymbol{\nu}(k+j-1|k)), j \in [1, N_p] \\ u_{\min} \le u(k+j|k) \le u_{\max}, \\ v_{\min} \le v(k+j|k) \le v_{\max}, j \in [0, N_p] \\ \boldsymbol{\nu}_{\min} \le \boldsymbol{\nu}(k+j|k) \le \boldsymbol{\nu}_{\max}, j \in [0, N_p - 1] \end{cases} \tag{22}$$

where $\boldsymbol{e}_0$ denotes the value of the system error obtained at the current time.

At each sampling time, the optimization problem (21) is solved, generating the optimal control sequence of the mobile robot velocity $\boldsymbol{\nu}^* = \{\boldsymbol{\nu}(k|k), \boldsymbol{\nu}(k+1|k), \cdots, \boldsymbol{\nu}(k+N_c|k), \cdots, \boldsymbol{\nu}(k+N_p-1|k)\}$.

From $\boldsymbol{\nu}(k+N_c+1|k)$ to $\boldsymbol{\nu}(k+N_p-1|k)$, the control input is equal to $\boldsymbol{\nu}(k+N_c|k)$ and is constant. The kinematic predictive stabilization control law is implicitly given by the first component of $\boldsymbol{\nu}^*$.

The objective of such a controller is to generate the desired velocity $\boldsymbol{\nu}_c = [\nu_c, \omega_c]^{\mathrm{T}}$ of the mobile robot for the dynamic controller.

3.2 Dynamic controller

The dynamic controller receives from the kinematic controller the desired linear and angular velocities $\boldsymbol{\nu}_c = [\nu_c, \omega_c]^{\mathrm{T}}$ which are obtained by (21), and generates the torque to make the velocity error between the actual velocity and the desired one asymptotically converge to zero. In this subsection, based on the dynamic model given by (3), a torque control law $\boldsymbol{\tau} = [\tau_1, \tau_2]^{\mathrm{T}}$ is designed to stabilize the system (15) and (3).

The dynamic model (3) can be rewritten as

$$\begin{cases} \dot{\nu} = \dfrac{\tau_1}{m} \\ \dot{\omega} = \dfrac{\tau_2}{I} \end{cases} \tag{23}$$

Applying the Euler′s approximation to (23), the discrete-time dynamic model of the mobile robot can be obtained as

$$\begin{cases} \nu(k+1) = \nu(k) + T\dfrac{\tau_1(k)}{m} \\ \omega(k+1) = \omega(k) + T\dfrac{\tau_2(k)}{I} \end{cases} \tag{24}$$

and (24) can be rewritten as

$$\boldsymbol{\nu}(k+1) = f(\boldsymbol{\nu}(k), \boldsymbol{\tau}(k)) \tag{25}$$

Based on (25), the predictive model can be formulated as follows:

$$\boldsymbol{\nu}(k+j|k) = f(\boldsymbol{\nu}(k+j-1|k), \boldsymbol{\tau}(k+j-1|k)), j \in [1, \bar{N}_p] \tag{26}$$

Define velocity error $\boldsymbol{\delta} = \boldsymbol{\nu}_c - \boldsymbol{\nu}$, then the quadratic objective function of the velocity error and control torque with a predictive horizon $\bar{N}_p$ and a control horizon $\bar{N}_c$ can be given by

$$\begin{aligned} \varphi(k) = & \sum_{j=1}^{\bar{N}_p} \boldsymbol{\delta}^{\mathrm{T}}(k+j|k)\bar{\boldsymbol{Q}}\boldsymbol{\delta}(k+j|k) + \\ & \sum_{j=1}^{\bar{N}_c} \boldsymbol{\tau}^{\mathrm{T}}(k+j-1|k)\bar{\boldsymbol{R}}\boldsymbol{\tau}(k+j-1|k) \end{aligned} \tag{27}$$

where $\bar{\boldsymbol{Q}}$ and $\bar{\boldsymbol{R}}$ denote symmetric positive definite weighting matrices. Furthermore, the torque limitation in (14) is considered.

Therefore, the following dynamic predictive controller can be obtained:

$$\boldsymbol{\tau}^* = \arg\min_{\boldsymbol{\tau}} \varphi(k) \tag{28}$$

s.t.

$$\begin{cases} \boldsymbol{\nu}(k|k) = \boldsymbol{\nu}_0 \\ \boldsymbol{\nu}(k+j|k) = f(\boldsymbol{\nu}(k+j-1|k), \\ \qquad\qquad \boldsymbol{\tau}(k+j-1|k)), j \in [1, \bar{N}_p] \\ \boldsymbol{\delta}(k+j|k) = \boldsymbol{\nu}_c(k) - \boldsymbol{\nu}(k+j|k), j \in [1, \bar{N}_p] \\ \boldsymbol{\tau}_{\min} \le \boldsymbol{\tau}(k+j|k) \le \boldsymbol{\tau}_{\max}, j \in [0, \bar{N}_p - 1] \end{cases} \tag{29}$$

where $\boldsymbol{\nu}_0$ is the value of the actual velocity at current time k, and we set the initial value $\boldsymbol{\nu}(0) = 0$.

At each sampling time, the constrained optimization problem (28) is solved, generating an optimal control sequence $\boldsymbol{\tau}^* = \{\boldsymbol{\tau}(k|k), \boldsymbol{\tau}(k+1|k), \cdots, \boldsymbol{\tau}(k+\bar{N}_c|k), \cdots, \boldsymbol{\tau}(k+\bar{N}_p-1|k)\}$.

From $\boldsymbol{\tau}(k+\bar{N}_c+1|k)$ to $\boldsymbol{\tau}(k+\bar{N}_p-1|k)$, the control torque is equal to $\boldsymbol{\tau}(k+\bar{N}_c|k)$ and constant. Only the first argument, $\boldsymbol{\tau}(k|k)$, is applied to generate the actual velocity of mobile robot using (24) and deliver the actual velocity to robot servos.

4 Simulation results

In this section, several simulations are implemented in Matlab to demonstrate the validity of the proposed control scheme, considering the robot′s physical parameters $m = 4\,\mathrm{kg}$ and $I = 2.5\,\mathrm{kg\cdot m^2}$. The simulated images are obtained through a virtual camera with a focal length $f = 6\,\mathrm{mm}$, and the size of the virtual images is 640×480 pixels. In our simulations, four static points are used as the target features. The initial pose of the mobile robot is $\boldsymbol{q}_0 = [1.5, -5, 0]^{\mathrm{T}}$ and the desired pose is $\boldsymbol{q}_d = [0, 0, 0]^{\mathrm{T}}$. The distance from the mass center of the mobile robot to the camera position is set to $l = 0.1$ m and the parameter α is selected as $\alpha = 5\mathrm{m}^{-1}$.

In all the presented simulations, the nonlinear constrained optimization problem is solved by the "fmincon" function. The sampling time T is selected as $T = 100\,\mathrm{ms}$, the prediction horizons are $N_p = 5, \bar{N}_p = 3$, and the control horizon $N_c = \bar{N}_c = 1$. The weighting matrices are chosen

as follows:

$$\boldsymbol{Q}=\begin{bmatrix}100&0&0\\0&100&0\\0&0&50\end{bmatrix},\quad \bar{\boldsymbol{Q}}=\begin{bmatrix}120&0\\0&120\end{bmatrix} \tag{30}$$

$$\boldsymbol{R}=\bar{\boldsymbol{R}}=\begin{bmatrix}0.1&0\\0&0.1\end{bmatrix} \tag{31}$$

and the control constraints are selected as

$$\begin{bmatrix}-3\,\text{m/s}\\-1.5\,\text{rad/s}\end{bmatrix}\le\boldsymbol{\nu}\le\begin{bmatrix}3\,\text{m/s}\\1.5\,\text{rad/s}\end{bmatrix} \tag{32}$$

$$\begin{bmatrix}-50\,\text{N}\cdot\text{m}\\-50\,\text{N}\cdot\text{m}\end{bmatrix}\le\boldsymbol{\tau}\le\begin{bmatrix}50\,\text{N}\cdot\text{m}\\50\,\text{N}\cdot\text{m}\end{bmatrix} \tag{33}$$

Simulation 1. The simulation is implemented for the controllers defined in (21) and (28) without considering the visibility constraints. The simulation results are shown in Fig. 2.

From Fig. 2 (a), we can see that the mobile robot is driven to the desired pose, which implies that the current image is convergent to the desired image, as shown in Fig. 2 (b). The corresponding behavior of the state of the mobile robot is presented in Fig. 2 (c). We can see that the state variables x, y, and θ are all convergent to the desired values. Fig. 2 (d) shows that the controller can correct the system error quickly (about 7.8 s) and the system error asymptotically converges to zero. The actual velocities, desired velocities, and torques obtained by the control algorithm are shown in Fig. 2 (e) $\sim$ (g). It is clear the presence of the control constraints that these control inputs tend to zero finally.

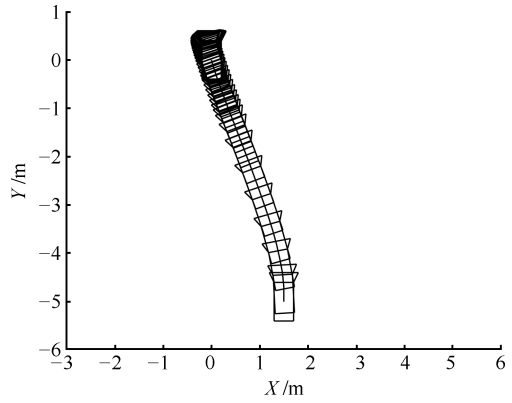

(a) Trajectory of the mobile robot on the X-Y plane

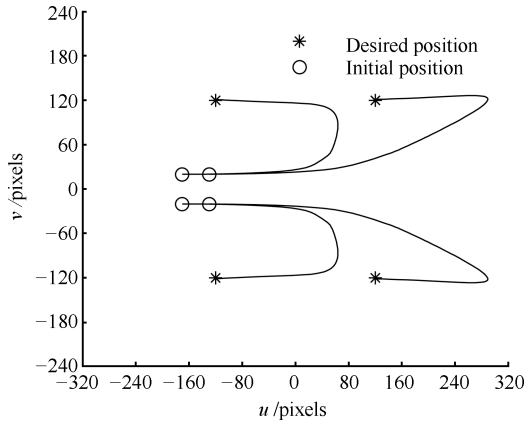

(b) Trajectories of the feature points in the image

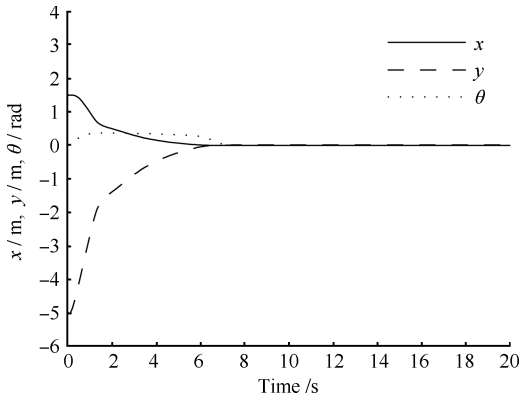

(c) State variables of the mobile robot

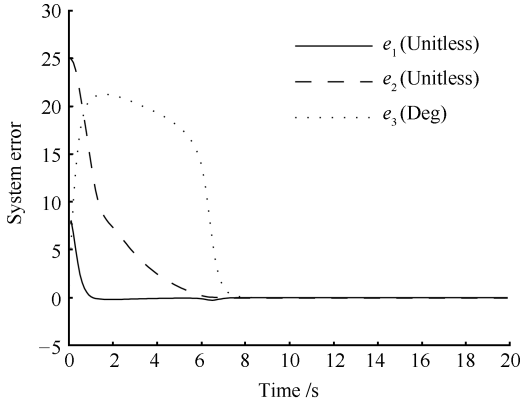

(d) System error e_1, e_2, e_3

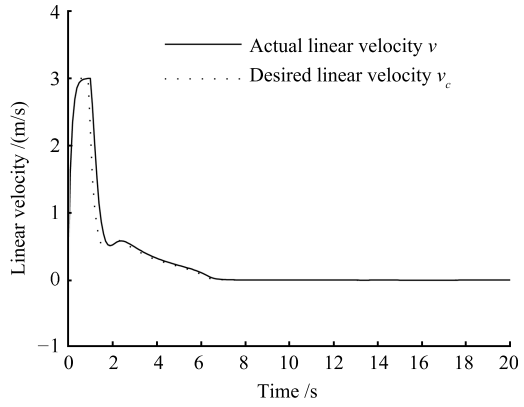

(e) Actual and desired linear velocities

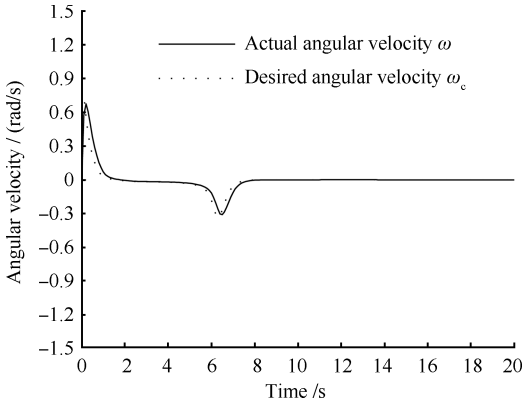

(f) Actual and desired angular velocities

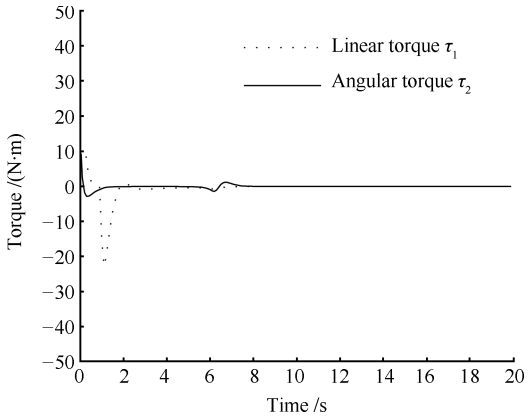

(g) Linear and angular torques

Fig. 2 Simulation results without visibility constraints

These results show the feasibility of the proposed approach. However, we can find that in Fig. 2 (b), two feature points are at the edge of the image plane during servoing process. When the control inputs increase or the robot is at other initial pose, these two feature points may move out of the image plane. For example, when the initial pose is selected as $\boldsymbol{q}_0 = [1.5, -3.5, 0]^{\mathrm{T}}$, we can observe that these two feature points escape beyond the camera field-of-view depicted in Fig. 3. In practical application, if some targets get out of the camera field-of-view during servoing process, the value of the current features can no longer be computed, which leads to the interruption of the control algorithm, i.e., the failure of servoing. Therefore, it is necessary to take the visibility constraints into account.

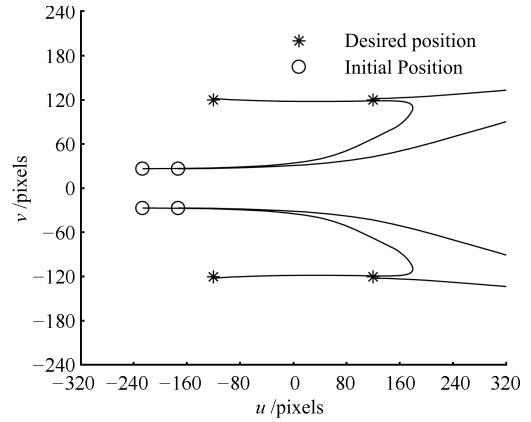

Fig. 3 Trajectories of the feature points in the image

Simulation 2. In order to demonstrate the capability of handling visibility constraints, the limitations in image pixel coordinates of feature points are now considered as follows:

$$\begin{bmatrix} u_{\min} = -240\,\text{pixels} \\ v_{\min} = -200\,\text{pixels} \end{bmatrix} \leq \begin{bmatrix} u \\ v \end{bmatrix} \leq \begin{bmatrix} u_{\max} = 240\,\text{pixels} \\ v_{\max} = 200\,\text{pixels} \end{bmatrix} \tag{34}$$

The simulation results are shown in Fig. 4.

As can be seen in Fig. 4 (a) and (b), the proposed controller allows to satisfy both the stabilization task and the visibility constraints. The robot trajectory on the motion plane is modified to ensure that the feature points do not get out of the field of view. The exponential behavior of the mobile robot state is presented in Fig. 4 (c). From Fig. 4 (d), we can observe that the system error can be corrected quickly and tends to zero asymptotically. Fig. 4 (e) ∼ (g) show the actual velocities, desired velocities and torques, respectively. We can note that the control signals are more smooth compared with the results in Simulation 1.

Simulation 3. To test the robustness of the proposed predictive controller, image noise with a standard deviation of 0.2 pixels is added to the feature points. Furthermore, a white noise distributed with amplitude of 0.02 is added to the control inputs. The simulation results are demonstrated in Figs. 5 ∼ 9. We can observe that the control objective can still be achieved with a quite small error despite the existence of the external disturbances.

Therefore, all of the simulation results demonstrate that the proposed control strategy is effective to solve the visual servo stabilization problem while handling constraints.

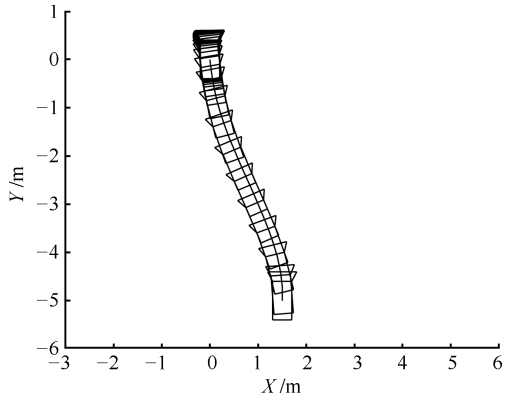

(a) Trajectory of the mobile robot on the X-Y plane

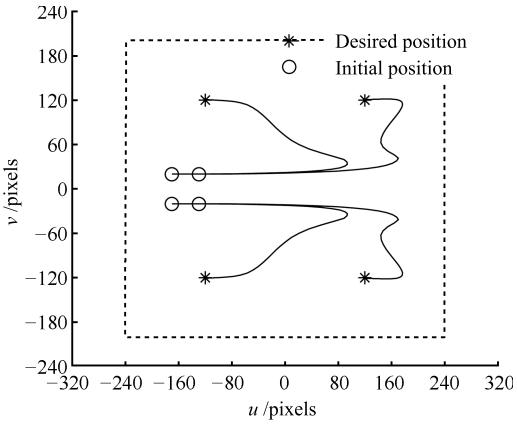

(b) Trajectories of the feature points in the image

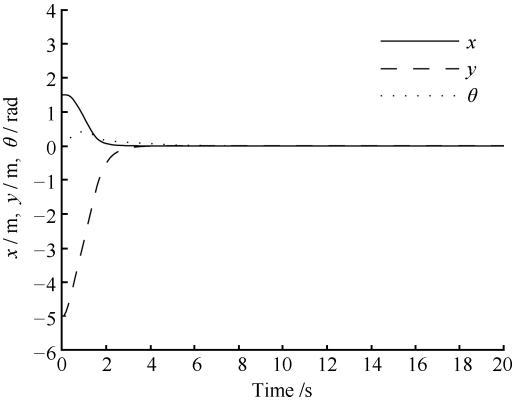

(c) State variables of the mobile robot

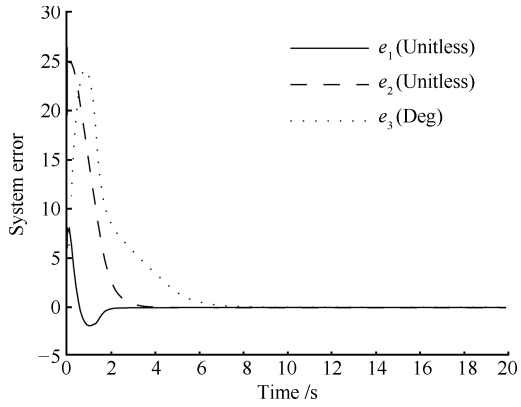

(d) System error e_1, e_2, e_3

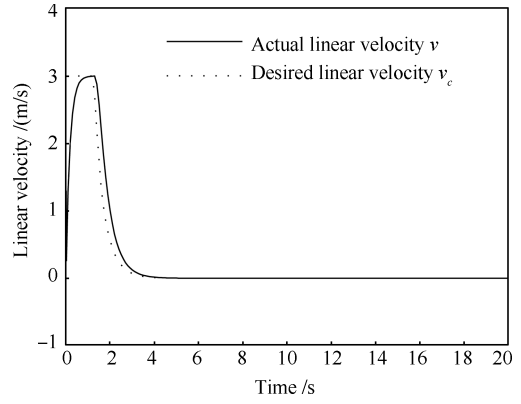

(e) Actual and desired linear velocities

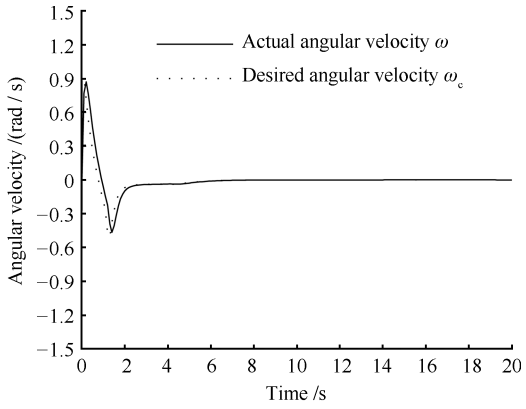

(f) Actual and desired angular velocities

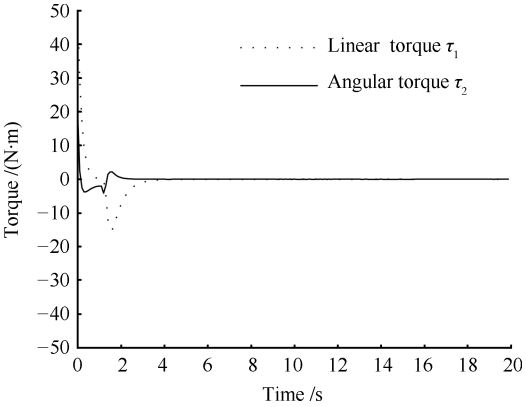

(g) Linear and angular torques

Fig. 4 Simulation results with visibility constraints

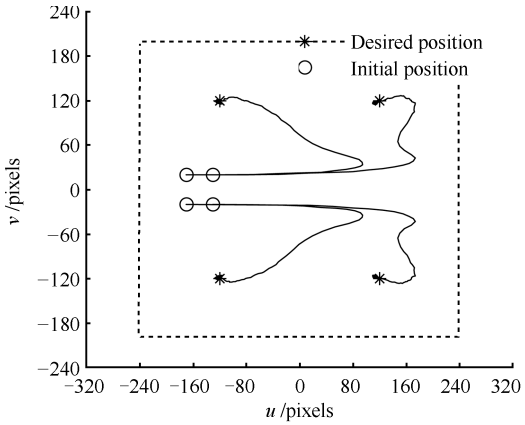

Fig. 5 Trajectories of the feature points in the image

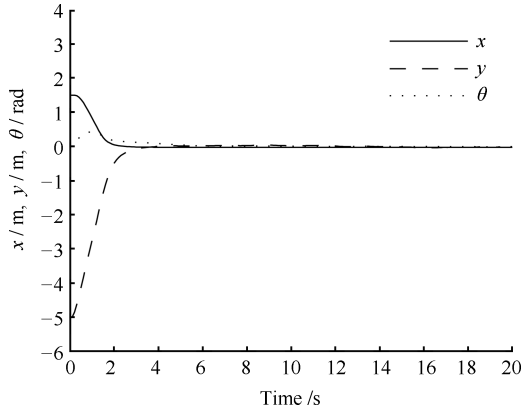

Fig. 6 State variables of the mobile robot

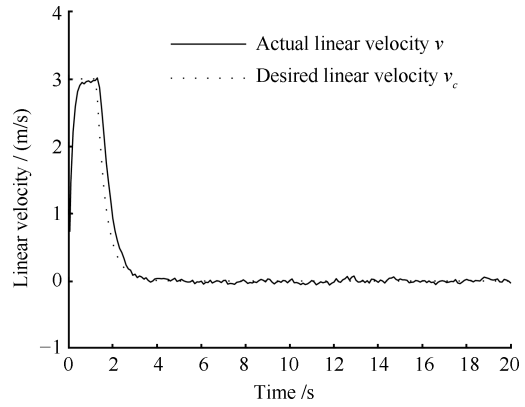

Fig. 7 Actual and desired linear velocities

5 Conclusions

Based on nonlinear model predictive control technique, a two-stage visual predictive stabilization controller, combining both the kinematic and dynamic controllers, has been proposed for a nonholonomic mobile robot. By expressing the control objective as an optimization problem, the visibility and control constraints are easily dealt with in the controller design. The designed predictive controller not only is capable of driving the mobile robot to the desired pose though the depth information is unknown, but also can keep the feature points always visible during the visual servo process. All the simulation results indicate that the proposed strategy is indeed feasible and effective.

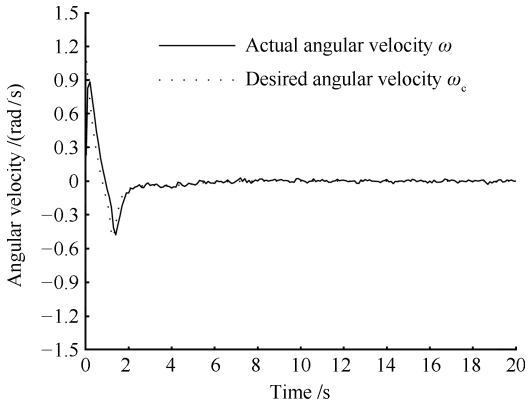

Fig. 8 Actual and desired angular velocities

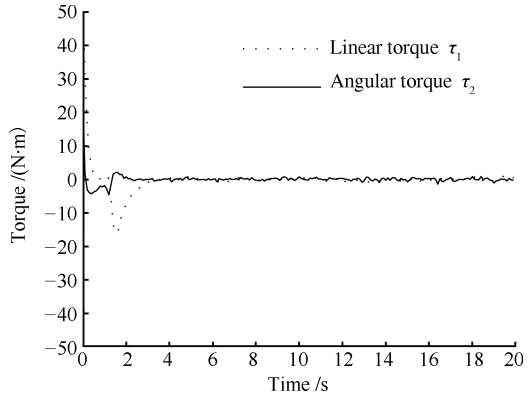

Fig. 9 Linear and angular torques

References

1 Wang Q D, Wei C L. Robust adaptive control of nonholonomic systems with nonlinear parameterization. *Acta Automatica Sinica*, 2007, **33**(4): 399−403

2 Hu Y M, Ge S S, Su C Y. Stabilization of uncertain nonholonomic systems via time-varying sliding mode control. *IEEE Transactions on Automatic Control*, 2004, **49**(5): 757−763

3 Marchand N, Alamir M. Discontinuous exponential stabilization of chained form systems. *Automatica*, 2003, **39**(2): 343−348

4 López-Nicolas G, Sagüés C, Guerrero J J, Kragic D, Jensfelt P. Nonholonomic epipolar visual servoing. In: Proceedings of the 2006 IEEE International Conference on Robotics and Automation. Orlando, USA: IEEE, 2006. 2378−2384

5 Mariottini G L, Oriolo G, Prattichizzo D. Image-based visual servoing for nonholonomic mobile robots using epipolar geometry. *IEEE Transactions on Robotics*, 2007, **23**(1): 87−100

6 Becerra H M, López-Nicolas G, Sagüés C. A sliding-mode-control law for mobile robots based on epipolar visual servoing from three views. *IEEE Transactions on Robotics*, 2011, **27**(1): 175−183

7 Fang Y C, Dixon W E, Dawson D M, Chawda P. Homography-based visual servo regulation of mobile robots. *IEEE Transactions on Systems, Man and Cybernetics, Part B: Cybernetics*, 2005, **35**(5): 1041−1050

8 Lopez-Nicolas G, Sagues C, Guerrero J J. Homography-based visual control of nonholonomic vehicles. In: Proceedings of the 2007 IEEE International Conference on Robotics and Automation. Roma, Italy: IEEE, 2007. 1703−1708

9 López-Nicolás G, Guerrero J J, Sagüés C. Visual control of vehicles using two-view geometry. *Mechatronics*, 2010, **20**(2): 315−325

10 López-Nicolás G, Guerrero J J, Sagüés C. Visual control through the trifocal tensor for nonholonomic robots. *Robotics and Autonomous Systems*, 2010, **58**(2): 216−226

11 Zhang X B, Fang Y C, Liu X. Motion-estimation-based visual servoing of nonholonomic mobile robots. *IEEE Transactions on Robotics*, 2011, **27**(6): 1167−1175

12 Liang Zhen-Ying, Wang Chao-Li. Robust stabilization of nonholonomic chained form systems with uncertainties. *Acta Automatica Sinica*, 2011, **37**(2): 129−142

13 Yang Fang, Wang Chao-Li. Adaptive stabilization for uncertain nonholonomic dynamic mobile robots based on visual servoing feedback. *Acta Automatica Sinica*, 2011, **37**(7): 857−864

14 Wang Z L, Liu Y H. Visual regulation of a nonholonomic wheeled mobile robot with two points using Lyapunov functions. In: Proceedings of the 2010 IEEE International Conference on Mechatronics and Automation. Xi′an, China: IEEE, 2010. 1603−1608

15 Allibert G, Courtial E, Chaumette F. Predictive control for constrained image-based visual servoing. *IEEE Transactions on Robotics*, 2010, **26**(5): 933−939

16 Chen C Y, Li T H S, Yeh Y C, Chang C C. Design and implementation of an adaptive sliding-mode dynamic controller for wheeled mobile robots. *Mechatronics*, 2009, **19**(2): 156−166

17 Mayne D Q, Rawlings J B, Rao C V, Scokaert P O M. Constrained model predictive control: stability and optimality. *Automatica*, 2000, **36**(6): 789−814

CAO Zheng-Cai Professor at the College of Information Science and Technology, Beijing University of Chemical Technology. He received his Ph. D. degree from Harbin Institute of Technology in 2005. His research interest covers sensor technology and intelligent control of robot. Corresponding author of this paper.
E-mail: giftczc@163.com

YIN Long-Jie Master student at the College of Information Science and Technology, Beijing University of Chemical Technology. He received his bachelor degree from Beijing University of Chemical Technology in 2010. His main research interest is intelligent control of robot.
E-mail: yinlongjie123@126.com

FU Yi-Li Professor at Harbin Institute of Technology. He received his Ph. D. degree from Harbin Institute of Technology in 1996. His research interest covers autonomous robot control, medical robotics, and virtual reality.
E-mail: meylfu@hit.edu.cn

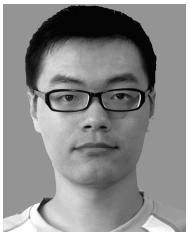

LIU Tian-Long Master student at the College of Information Science and Technology, Beijing University of Chemical Technology. He received his bachelor degree from Harbin University of Science and Technology in 2009. His research interest covers intelligent control of robot and biomimetic robots.
E-mail: spurtltl@126.com